ANNALS of Faculty Engineering Hunedoara
– International Journal of Engineering
Tome XV [2017] – Fascicule 2 [May]

ISSN: 1584-2665 [print; online]
ISSN: 1584-2673 [CD-Rom; online]
a free-access multidisciplinary publication
of the Faculty of Engineering Hunedoara

[1,2.]S.A. BELLO, [1.]J.O.AGUNSOYE, [1,3.]J. A.ADEBISI,
[1.]J. E.ANYANWU, [1.]A. A. BAMIGBAIYE, [1.]S. B.HASSAN

POTENTIAL OF CARBONISED COCONUT SHELL AS A BALL-MILLING INTERFACE FOR SYNTHESIS OF ALUMINIUM (1XXX) NANOPARTICLES

[1.] Department of Metallurgical and Materials Engineering, University of Lagos, Akoka, Yaba, Lagos, NIGERIA
[2.] Department of Materials Science and Engineering, Kwara State, University, Malete, Kwara State, NIGERIA
[3.] Department of Metallurgical and Materials Engineering, University of Ilorin, Ilorin, NIGERIA

Abstract: Synthesis of Al (1xxx) nanoparticles (Alnp) for polymer reinforcement has been presented. Carbonized coconut shell (CCSs) was used as solid interface/lubricant for ball-milling synthesis. Particle behaviour through FT-IR and XRD was studied. Scherrer's theoretical size calculation and SEM/TEM imaging sizes were performed on Alnp obtained at varied milling durations. Results obtained indicated a shift in infrared transmittance peaks and an increase in correlative intensities signifying elastic deformation-induced breakage of Alnp which caused their greater counts as the milling in progress. A minimum crystallite size (3.56 nm) implies that the minimum breakage (threshold) level of Alnp was reached at 46 hours. However, further milling up to 70 hours assisted in the size reduction of the coarse Alnp but agglomeration of the finest ones also occurred owing to Vandal Waal's attraction resulted from increasing particle surface energy. This was ascertained by bigger size (22.89 nm) of the finest Alnp obtained at 70 hours. A phase inconsistence observed from XRD patterns can be linked with the blockage of reflected rays from extremely fine phases of Alnp by relatively coarse nanocrystalline phases. XRD, SEM and TEM indicated a decrease in Alnp sizes with an increment in milling duration.
Keywords: Al (1xxx); transmittance; Ball-milling; Precursor; Nanoparticles

1. INTRODUCTION

A high interest has been made on the synthesis of aluminium nanoparticles forpolymer reinforcement. High production rates and requirement of less expensive equipment found a basis of preference for ball milling over other techniques for metal particle production. Ball-millinginvolves crushing and breaking of micro particles mechanically in rotating drum known as vial by hardened steel, tungsten carbide, yttrium stabilized zirconia (YBZ)or alumina balls. Mechanical stresses produced from collisions of the milling balls act on the particles resulting in theirfragmentation into smaller oneswhen the stress intensity factor of the balls exceeds the fracture/impact toughness of the particles(Perez, 2004). Studies on ball-milling synthesis are common and reported in literatures(Chauruka et al., 2015; Loh et al., 2015;Qu et al., 2015). It has been established on particle miniaturization via the ball milling that once a certain small particle (threshold)size is reached, further milling causes no particle breakage but particle-particle interaction due to high particle surface energy, leading to particle welding/reintegration (Bello et al., 2015). Several explanations have been offered to support occurrence of the ball-milled particle thresholdsize, such as that of (Eckert et al., 1992; Hanna et al., 2014) who attributed the particle threshold size to balances between formation of dislocation and its recovery by thermal process. Also, minimum particle size of the nanocrystalline material obtained through mechanical attrition was modelledand result indicated a decrease in threshold size with the particle hardness but an increase with stacking fault and exponential function of activation energy(Mohamed, 2003).

For synthesis of nanoparticles from ball-milling, parameters such as milling durations, charge ratio, size of the initial powder, ball materials, ball sizes, filling level of the vialand the powder properties are very significant. Milling durations between 15 and 100 hours have been reported by different authors (Bello

et al., 2015; Breitung-Faes and Kwade, 2008; Eckert et al., 1992; Hanna et al., 2014; Janot and Guérard, 2005; Knieke et al., 2010; Mazaheri et al., 2010) for nanoparticles synthesis but different % particle pollution due to surface attrition of the balls has been reported. Janot and Guérard, (2005) reported 0.1-1% impurity in the dry ball milling study on lithium intercalation into graphite between 24 and 96 hours of milling using 5-10 mm hardened steel balls. When the ball size increased to 20 mm within the same milling interval, the particle pollution rose to 1-3 %. Synthesis of coconut shell nanoparticles between 16 and 70 hours at 10 charge ratios was achieved from initial powder of 37 µm(Bello et al., 2015). Also, Al 6061 nanoparticles were synthesized by (Hanna et al., 2014) from 56 µm Al 6061 powder through 15 hours cryogenic milling. Charge ratio is the mass of the milling balls divided by mass of the powders(Bello et al., 2015). It is an important parameter thatdetermines frequency of the shock received by the individual powders under milling process. A very high charge ratio simply means that the milling is energetic and the shock intensities are very high. High energyball milling can cause rapid fracture of the particle, thereby minimizing the milling duration for obtaining nanoparticles but particle amorphitization and high temperature are challenges. Review on mechanical milling by (Prasad Yadav et al., 2012) shows local warming temperatures between 50 and 215˚C reported by different authors. It has been established by (Eckert et al., 1998) that the temperature due to high energy ball milling can reach 400 ˚C and this temperature is homogeneous because of the continual rotation of the drum/vial (Maurice and Courtney, 1990). The local warming softens the particles and enhances their impact absorbing properties. This causes inelastic deformation instead of particle fracturing. Therefore, optimization of milling duration and charge ratio is necessary. In addition, vial filling level is directly proportional to the charge ratio. To enhance ball impact on the particles, vial should be as high as 80-90 % free(Janot and Guérard, 2005).

Properties of the powders under milling such asinitial powder size, hardness/brittleness and ductility determine the behaviour of the powders. Hardness/brittleness of the heavy metals favours their breakages. However, low melting metal (Al) powders are very ductile and seem to absorb ball impacts causing their flattening instead of breakages. Upon this, cooling of the Al powders is necessary during ball-milling. Both wet and cryogenic millings have solved cooling requirement of the ductile Al powdersduring ball milling(Breitung-Faes and Kwade, 2008; Essl et al., 1999; Hanna et al., 2014; Kwade, 1999; Shonhiwa et al., 2009; Watson et al., 1998; Zhang et al., 2015) but complete nitrogen/dodecaneremoval from the particle surfaces after synthesis is a great task.

In this present work, milling behaviour of Al (1xxx)had been studied. The work was aimed at studying suitability of CCSsas a ball-milling interface for improving the breakage of Al (1xxx). Effects of milling durationson Alnp size and morphology were also examined. Previously, authors have reported some studies on ball-milling synthesis(Bello et al., 2106; Bello et al., 2015; Bello et al., 2015;Hassan et al., 2015). Al (1xxx) is very light, ductile and 99 % pure. Little or nothing is knownon their nanoparticle ball-milling synthesis using CCS lubricant/ball-milling interface. Therefore, this attempt is novel, worthy of study and supports the global recycling/cost effective strategy and the synthesis of soft/light reinforcement materials for fabrication of high performance composites for aerospace and automobile applications (Department of Transportation National Highway Traffic Safety Administration, 1990; Fredriksson et al., 2010; The United Kingdom Composites Industry, 2013). Impregnation of Alnp in polymer for high performance composite development is currently ongoing and will form part of another article in future.

2. MATERIALS AND METHODOLOGY

The coconut shells (CSs)and Al cans used in this study were obtained within Lagos State, Nigeria. 500 g ofCSs were rinsed in water and dried in a Uniscope Laboratory oven (Model/serial no: SM 9053/1302271; ±1˚C precision) at 150˚C for 6 hours. The driedCSs were broken into pieces using hammer crusher (Model/serial no: 000T/13634), placed inside a cylindrical stainless steel crucible and sealed. Heating was carried out up to 1000˚C at 5˚C/min in a flowing argon stream using Carbolite tube furnace (Model: CTF 17/…/600) and held at this temperature for 2 hours before furnace cooling to ambient temperature. Al cans were re-melted and cast into a cylindrical bar using a sand mold. Elemental analysis of the Al cast reveals 99% purity(Bello et al., 2015). The castwas split into pieces using Colchester/triumph lathe machine (model: 2000). During splitting, the cast surface was cooledintermittently via water jets. Before ball-milling, theAl(1xxx) pieces were further broken manually using a hardened steel mortar and pestle. The pieces/CCSs stoichiometric mass ratio 100:1; and the pieces/balls ratio 17:2 were adopted for ball-milling using 87002 LIMOGES planetary mill (model: 28A20-92) with a mixture of ceramic balls (5-30 mm) at 192 rpm vial rotational speed. Initially,

CCSs were milled for 30 min for balls surface coating. Then, Al (1xxx) pieceswere added, milled for 40 hours and discharged. Vial was tightly sealed before every milling exercise. The milled powders were classified using a set of sieves in a descending order of grain fineness (2000-75 µm), vibrated mechanically for 30 minutes with the aid of a sine shaker. The finest Al (1xxx) powders collected in a pan below75µm sieve were used as a precursor for Alnp synthesis.

Precursor was further milled using the same charge ratio (17:2) for additional 70 hours (post classification). Samples taken at 16, 46 and 70were analyzed. Peaks, chemical bonds/functional group and intensities of phases characterizing the milled Alnp and CSs before and after carbonization were investigated using Shimadzu Fourier transform infrared spectroscopy, FT-IR (Apodization: Happ-Genzel). A pressed disc technique according to (Brian et al., 1989) was used in the sample preparation. Each sample was scanned at transmittance ranges from 500 to 4000 cm^{-1}at 4 cm^{-1} resolutionsfor 45 times for accuracy of the spectrum. Phases identification was studied using Empyrean X-ray diffractometer (XRD). The slits were fixed with Fe filtered Co $K\alpha_{\lambda= 1.79nm}$radiation.X'Pert High Score software; PAB-ICSD and ICCD (2014) data bases were used for phase identification. Particle morphology was examined using ASPEX 3020 scanning electron microscope, SEM (Model: SIRIUS 50/3.8) and Veletatransmission electron microscope (TEM). Theoretical size determination through XRD aided Scherrer's equation was compared with imaging sizes obtained from SEM and TEM aided with Gwyddion software.

3. RESULTS AND DISCUSSION

3.1. FT-IR spectrographs of aluminium (1XXX) nanoparticles

Peaks predicting the bond and functional groups of various phases of the precursor, Alnp and CSs are presented on Figure 1. Various peaks on curves a-b of the precursorand Alnpobtained at 70 hours post classification (PC) milling were assigned with bonds and functional groups as shown on Table 1, in accordance with (Brian et al., 1989). Bonds on Table 1 justifies the presence of organic compounds which can be classified aromatic amine and mercaptans both in precursor and Alnp. Presence of these compounds may be ascribedto CCSs used as ball-milling interface/lubricant. All phases characterizing the Alnp have stronger intensities than those of the precursor. The difference observed in the intensities could be attributed to breakage of precursor phasesto smaller ones of Alnp having greater counts. This supports the literature(Pokropivny et al., 2007).

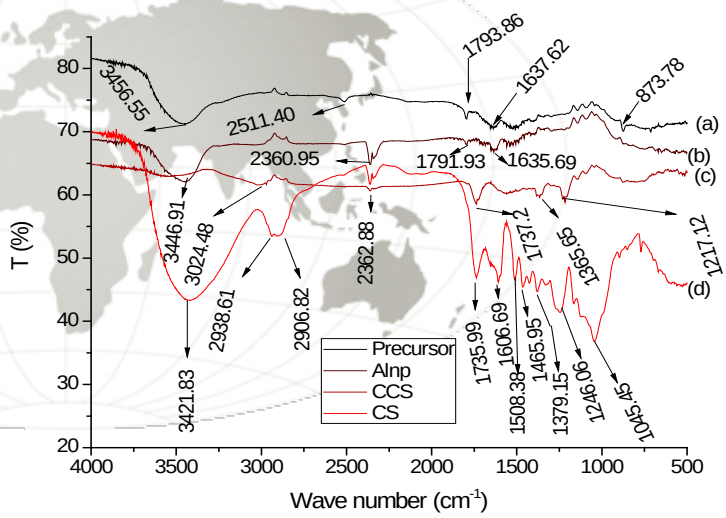

Figure1: FT-IR spectrographs of milled Al (1xxx) particles

Table1: Assignments of bonds/functional groups to Al (1xxx) particle FT-IR peaks

Order	Precursor	Alnp	Precursor	Alnp	Bond	Functional group
	Peaks (cm^{-1})		Corr. intensities			
1	3456.55	3446.91	0.010	0.105	N-H^{w} stretch	N-H (2°amine)
2	2511.40	2360.95	0.799	2.267	S-H stretch	S-H (mecarptans)
3	1637.62	1635.69	0.419	0.485	C-C^{m} stretch	C-C (aromatics)
4	873.78	-	1.403	-	C-H^{s}	C-H oop (aromatics)
5	650.03	635.69	0.154	0.394	C-Br^{w}	Alkyl halide
Key	^{s} = strong; ^{m} = medium; ^{w} = weak, oop = out of plane					

Absence of Al peaks may be attributed to its non-absorption/transmittance of infrared rays within the frequency (wave number) ranges used for particles analysis. The range (500-4000 cm^{-1}) greater thanKBrabsorption/transmittance frequency range (2 -25 µm) confirmedKBr non-interferencewith FT-IR spectrographs on Figure 1. Table 2 shows the bonds and functional groups of peaks on curves c and d representing CCSs and uncarbonised CSs. Confirmation of aliphatic, aromatic and amine compounds justifies the presence of cellulose, lignin, pentosans/holocellulose and uronic anhydrides in the CS. However, during vacuum carbonization, most of those compounds distilled off through the process of dehydrogenation/denitrogenation occurring within 1000°C. This accounts for smaller intensities of

phases of CCSs, disappearance of some existing and formation of new bonds as shown on Table 2. Therefore, curve c appeared different from curves a and b due to presence of Al (1xxx) as the major particles and their disintegration into smaller pieces due to ball milling.

Table2: Ascription of bonds/functional groups to CS particle FT-IR peaks

Order	CS	CCS	CS	CCS	Bond	Functional group
	Peaks (cm^{-1})		Corr. Intensities			
1	3421.83	-	0.057	-	N-H stretch	N-H (secondary amine)
2	2939.61	-	0.926	-	CH_2 asymmetric	Alkane
	-	3024.48		0.0215	C-H stretch	Aromatics
3	2906.82	-	0.968	-	C-H stretch	Alkane (sp^3)
4	1735.99	1737.2-	7.641	1.0099	C=O stretch	Aldehydes
5	1608.69	-	5.084	-	C-C stretch	Aromatics
6	1508.38	-	5.155	-	N-O asymmetric stretch	Nitro compounds
7	1379.15	-	2.55	-	$C-CH_3$	Alkane
8	-	1365.65	-	0.4056	C-H rock	Alkane
9	-	1217.12	-	0.8979	C-H wag	Alkyl halide
10	1246.06	-	2.216	-	C-N stretch	Aliphatic amine
11	1045.45	-	7.174	-	C-N stretch	Aliphatic amine
Key	^{s} = strong; ^{m} = medium; ^{w} = weak					

3.2. X-ray diffractometry of aluminium (1XXX) nanoparticles

Influence of ball milling using CCSs as the milling interface on the precursor with an increment in milling duration is shown on Figure 2a-c. Presence of Al_2O_3, Al and (Na, Ca) Al(Si Al)$_3O_8$ (albite/calcian) was observed on Figure 2a. On Figure 2b, only two phases, Al_2O_3 and Al were detected while on Figure 2c, Al_2O_3; Al and SiO_2 were confirmed. The phase inconsistence observed as the milling duration increased can be associated with repeated deformation of the precursor powders due to progressive ball shocks/impacts. During this process, albian and calciancrystalswere broken down into extremely fine particles such that during XRD analysis, rays reflected by albian and calcian tiny crystals were interrupted/blocked by SiO_2, Al and Al_2O_3 having larger crystals causing their non-detection.This agrees with literature(Li et al., 2001). Oxides can be attributable to unavoidable chemical interaction of phases of Al (1xxx) particles with CCSs/milling atmosphere and or surface cooling water jets. This reaction can be prevented through application of cryogenic nitrogen/dodecane(Hanna et al., 2014) but their complete removal from particle surface is impossible(Janot and Guérard, 2005). Presence of nanocrystalline oxides within Alnp is not a detriment since it will enhance Alnp polymer reinforcement tendency.A reduction in the peak numbers observed on Figure 2a-c depicts amorphitization of the phases. Therefore, Alnp appeared in a state, devoid of long periodic order of atomic arrangement known as quasicrystal state. This pars with literatures (Liu et al., 2013; Yang et al., 2015; Zhang et al., 2015;Zhang et al., 2015). Moreover, peak broadness justifies a decrease in Alnp sizes. This is on a par with FT-IR result.

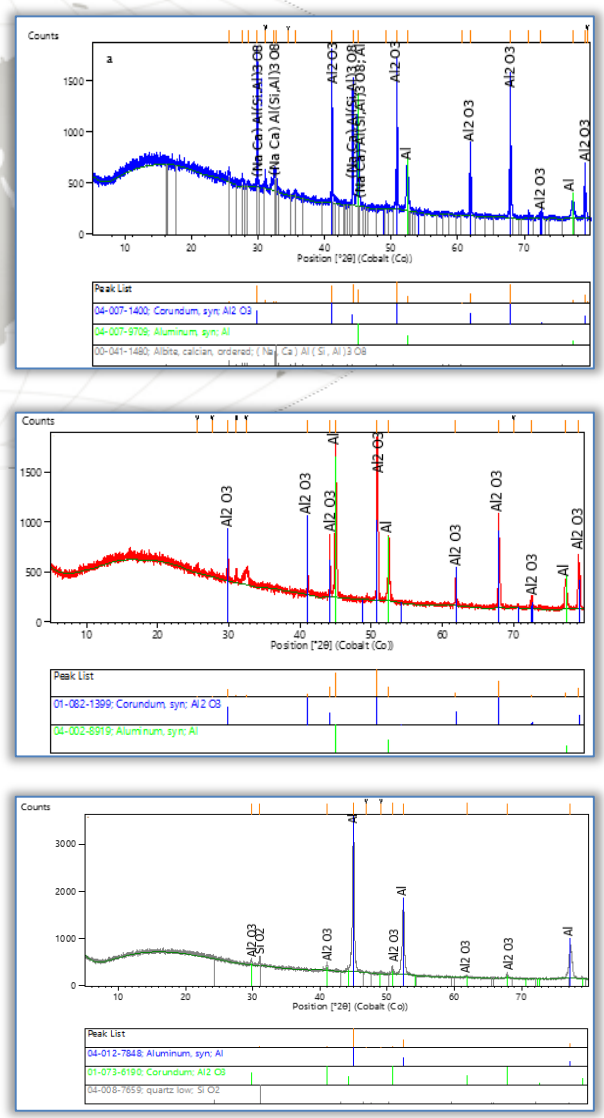

Figure2: XRD profiles of the Al (1xxx) at (a) 16, (b) 46 (c) 70 hours of post classification milling

However, Alnp size determination from XRD aided with Scherrer's equation (Bello et al., 2015; Speakman, [n,d]) indicated minimum sizes of 6.58, 3.56 and 22.89 nm at 16, 46 and 70 hours respectively. The respective maximum sizes are 857.44, 129.54 and 103.11 nm while the average sizes are 109.55, 70.17 and 55.50 nm respectively. Minimum size of 3.56 nm implies the attainment of finest Alnp at 46 hours milling (PC). Reintegration of the finest Alnp as the cyclic deformation through ball milling progressed could be responsible for a greater size of the finest Alnp obtained at 70 hours. The minimum size (3.56 nm of Alnp) at 46 hours could be attributed to balance between formation of dislocation (strain hardening) and recovery of the dislocation by inelastic deformation induced local warming(Eckert et al., 1992; Mohamed, 2003). Smallest average size of Alnp found at 70 hours affirms domination of particle breakage over agglomeration during ball milling synthesis. Therefore, ball milling synthesis is actually a particle miniaturization technique for producing metallic and nonmetallic metallic particles. This supports(Wolff et al., 2014).

3.3. SEM morphology of aluminium (1XXX) nanoparticles

Morphology of CCS interface between milling balls and precursor during synthesis is presented on Figure 3.

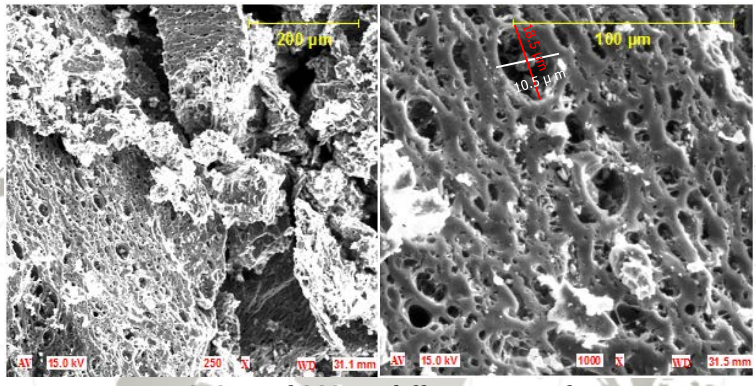

Figure 3: SEM of CCSs at different magnifications

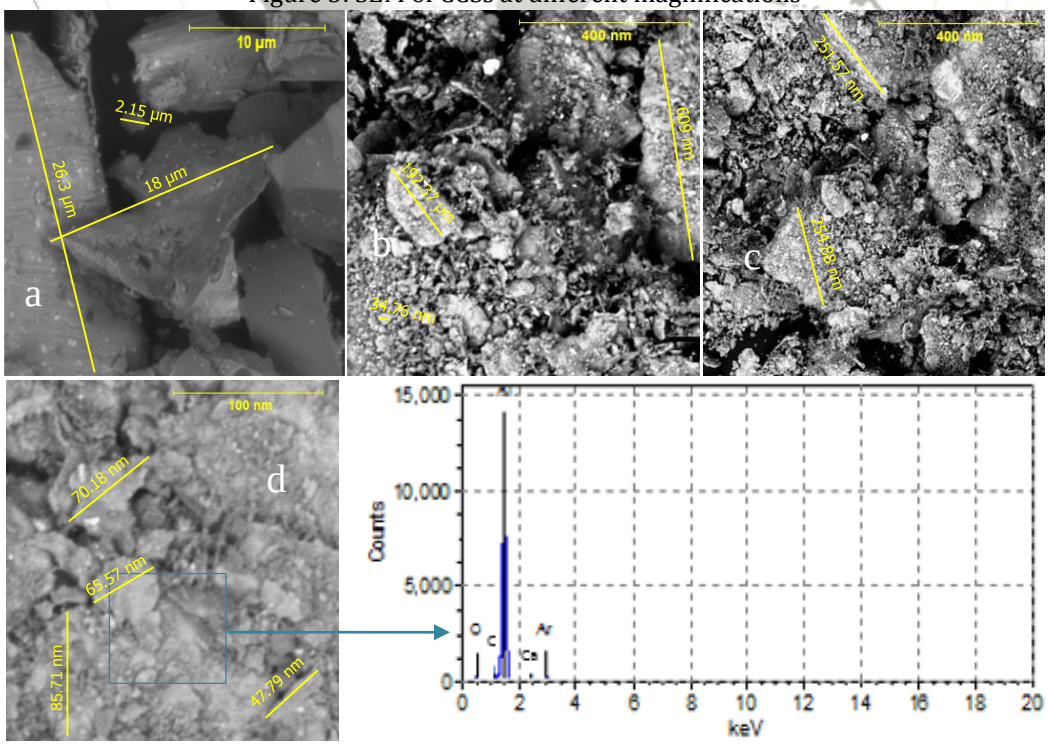

Figure4: SEM of (a) precursor (b) Alnp at 16, (c) Alnp at 46 hours
(d) with EDX of Alnp at 70 hours (post classification) milling

The microstructures at different magnifications revealed layered structures having sheets of graphitic carbon. The layered structures are indices for CCS lubrication. Each layer contains numerous vacancy imperfections having micro voids of varied orientations and sizes. The measured sizes of one of the voids at the top layer are 18.5 and 10.5 µm respectively. Formation of these voids can be linked with various paths taken by the volatiles in diffusing out of the CSs during carbonization. Presence of voids within CCSs aided their breakage during the prime milling to coat the surface of the balls. The CCS powder acted

as an interface to prevent the sticking of the milled precursor particles to the surface of the milling balls. This reduced particle inelastic deformation and enhanced the fracturing of the particles. Chemical reaction of phases of CCSs and precursor particles during the course of milling resulted in the formation of hard and relative brittle phases (see Figure 2) which reduced the impact absorbing properties of the precursor particles and caused improvement in their breaking tendency.

Micrograph on Figure 4a displays the morphology of the precursor particle. The observed particles are irregular in shape with dull appearance. The tiny white particles dispersed randomly within precursor particlescould be linked with CCS diffusioninto the precursor during the milling process. Figure 4b-c show the configuration of Alnp obtained at 16, 46 and 70. Each of the microstructures on Figure 4 reveals numerous domains consisting of many Alnp which had been welded or fused together by Vandal Waal's attraction due to increased surface energy during particle miniaturization. However, textural and appearance differences are very noticeable from one micrograph to another. This may be ascribed to transformation of phases of Alnp into new ones due to progressive/repeated plastic deformation from the ball impacts. During the process of plastic deformation, particle miniaturization occurred along with refinements of particle grains leading to formation of numerous grain boundaries. Barriers to dislocation movements by grain boundaries and hard phases (see Figure 2) increased the strain hardening of nanocrystalline particles and enhanced their breakages. Thermal conductivity of CCS (graphite) particles within the precursor grains assisted in the transfer of unavoidable heat generated from inelastic deformation of the particles. This reduced the rate of dislocation recovery that could set in due to increasing local warming. The dominance of strain hardening over recovery is a possible reason behind the breakage of the precursor powders to produce Alnp. Influence of ball milling and effectiveness of CCSs are very glaring on Figure 4a-d. All particles featuring in the micrograph on Figure 4a are big and can easily be identified from one another. Those big particles broke down into various smaller ones which existed inAlnp colonies with different degrees of agglomeration. Manual random size estimation from SEM revealed a range from 2.15 to 26.3 µm of the precursor on Figure 4a while respective sizes of a small and a big Alnp obtained at 16 hours were 34.75 and 609 nm (see Figure 4a-b).A very large difference between sizes of precursor particles and Alnp justifies particle size reduction through effectiveness of CCSs as a lubricating interface between the milled particles and the milling balls. The elemental study on Figure 4d indicated presence of Al, C, O, Ca and Ar. The elements except Araffirms various phases observed from XRD results (see Figure 2). Arcould be linked with Ar used as inert shield against the oxidation during carbonization of CSs.

3.4. TEM images of aluminium (1XXX) nanoparticles

It was observed from TEM images on Figure 5a-c that there were extremely fine particles surrounding the central large one which probably represented a relatively coarse Alnp. The big particle on Figure 5a was pilled due to progressive attrition by the ball impacts. Wear debris and agglomeration of extremely fine particles accounted for relatively large particles beside and around the central big one on Figure 5b-c respectively. The plastic deformation induced breakage continued as the milling duration increased, resulting in the smaller appearance of the central Alnp on Figure 5c than those on Figure 5a-b.

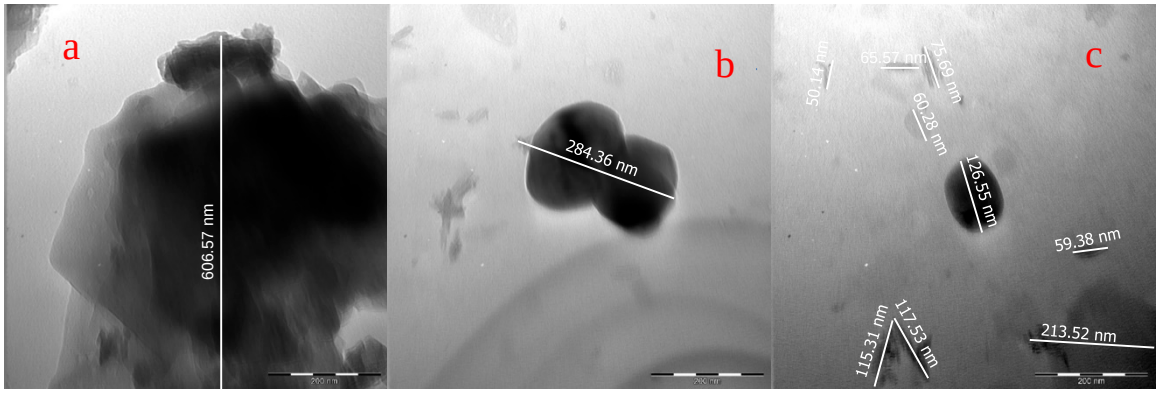

Figure 5: TEM images of Al (1xxx) nanoparticles (a) 16 hours, (b) 46 hours
(c) 70 hours (post classification) milling

Manually measured maximum sizes of Alnp on Figure 5a-c, are 606.57, 284.36 and 213.53 nm at 16, 46 and 70 hours (PC) milling respectively. However, automatic size determination from SEM/TEM supported with Gwyddion software revealed a size range between 0 and 0.61 µm at 16 hours; 0 and 254.9 nm (SEM); 0 and 284.4 nm (TEM) at 46 hours while 10 and 87.2 nm (SEM); 0 and 214 nm (TEM)

at 70 hours as shown on Figure 6a-c respectively. The corresponding average sizes from both SEM and TEM were matched with those obtained from XRD on Figure 7. The trend from Figure 7 is a decrease in Alnp average sizes with an increment in the milling duration. This shows consistence of XRD, SEM and TEM in the size determination. However, smaller XRD sizes than those of SEM and TEM affirmed the average crystal size determination by XRD while both SEM and TEM measured actual particle sizes. Since a particle may consist more than one crystal, particle sizes are expected to be greater than those of crystals (see Figure 8a). However, the slight difference betweenSEM and TEM average sizes could be linked with variations in the operational modes of both SEM and TEM which enabled them to present Alnp in different forms as shown on Figure 4 and Figure 5. The wide difference between maximum and minimum Alnp sizes as shown on Figure 6a-bmay be ascribed to active and dead milling zones occurred within the grinding media (see Figure 8b). The dead zone acted as particle hideout. Those particles within the dead zone at every instance of milling duration were out of point of tangential collisions between two balls. Therefore, no meaningful deformation of the particles within the dead zoneoccurred while the continual breakage was in progress in the active zone.

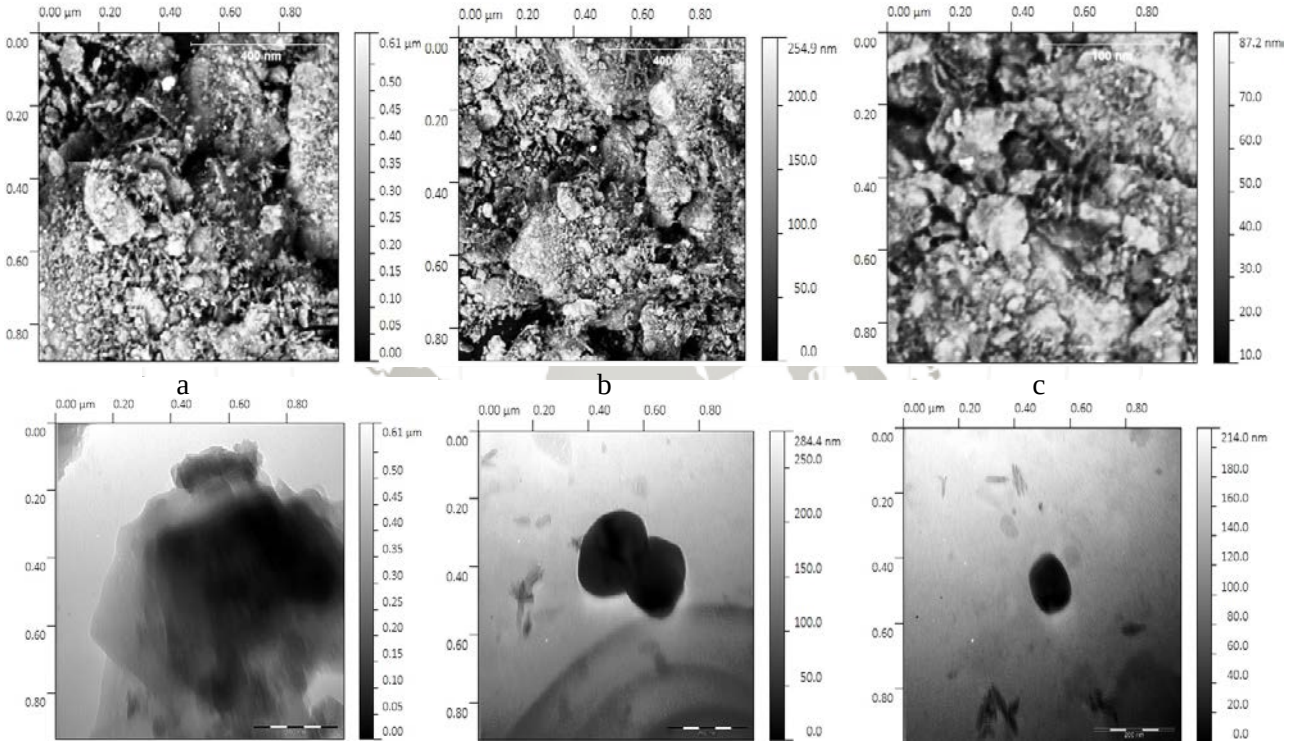

Figure6: SEM/TEM aided software size of Alnp (a) 16 (b) 46 (c) hours (post classification) milling

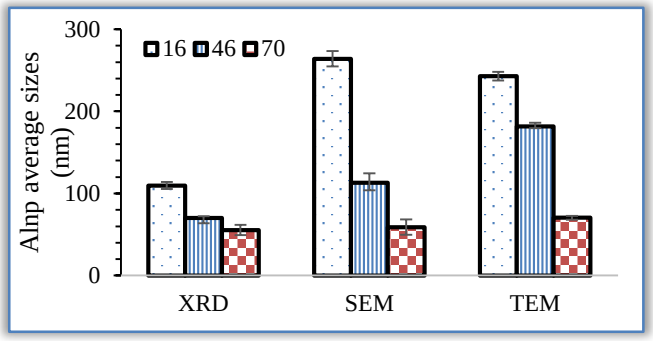

Figure 7: Alnp average sizes

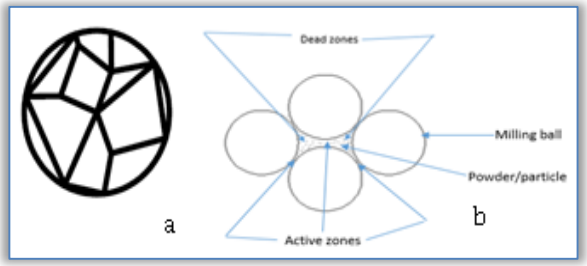

Figure 8: (a) Particles having more than one crystal (b) grinding media

4. CONCLUSION

Finally, Synthesis of Alnp via ball-milling was successful and CCS as a ball-milling interface was very effective. An average crystallite size of 55 nm was obtained at 70 hours post classification milling. Presence of micro void imperfection within CCSs aided their breakage for effective surface coating of the milling balls. There was a consistence in the theoretical size calculation and imaging measurement technique. The synthesized Alnp will be used as polymer reinforcement for development of advanced composites for automobile applications.

Acknowledgement
Authors appreciate Ceramics Department of Federal Industrial Institute of Research Oshodi (FIIRO) and Mrs Bello A. A. for their assistance in making this work a reality.

References

[1.] Bello, S. A., Agunsoye, J. O., Adebisi, J. A., Kolawole, F. O. and Suleiman, B. H.: Physical Properties of Coconut Shell Nanoparticles. Kathmandu University Journal of Science, Engineering and Technology, 12(1), 63-79. (2106).
[2.] Bello, S. A., Agunsoye, J. O. and Hassan, S. B.: Synthesis of Coconut Shell Nanoparticles Via A Top Down Approach: Assessment of Milling Duration on The Particle Sizes and Morphologies of Coconut Shell Nanoparticles. Materials Letters, 159, 514-519. (2015).
[3.] Bello, S. A., Hassan, S. B., Agunsoye, J. O., Kana, M. G. Z. and A, R. I.: Synthesis of Uncarbonised Coconut Shell Nanoparticles: Characterisation and Particle Size Determination Tribology in Industry, 37(2), 257-263. (2015).
[4.] Bello, S. A., Raheem, I. A. and Raji, N. K.: Study of tensile properties, fractography and morphology of aluminium (1xxx)/coconut shell micro particle composites. Journal of King Saud University - Engineering Sciences. (2015).
[5.] Breitung-Faes, S. and Kwade, A.: Nano particle production in high-power-density mills. Chemical Engineering Research and Design, 86(4), 390-394. (2008).
[6.] Brian, S. F., Anthony, J. H., Peter, W. G. S. and Austin, R. T. (1989). Textbook of Practical Organic Chemistry (5th ed., pp. a-1540). New York: John Wiley& Sons.
[7.] Chauruka, S. R., Hassanpour, A., Brydson, R., Roberts, K. J., Ghadiri, M. and Stitt, H.: Effect of mill type on the size reduction and phase transformation of gamma alumina. Chemical Engineering Science, 134, 774-783. (2015).
[8.] Department of Transportation National Highway Traffic Safety Administration. (1990). Laboratory Test Procedure for Regulation Part 581 Bumper Standard Safety Assurance.
[9.] Office of Vehicle Safety Compliance Room 6115, NSA-30 400 Seventh Street, SW Washington, DC 20590: United State of American.
[10.] Eckert, J., Holzer, J. C., Krill, C. E. and Johnson, W. L.: Structural and thermodynamic properties of nanocrystalline fcc metals prepared by mechanical attrition. Journal of Materials Research, 7(7), 1751-1761. (1992).
[11.] Eckert, J., Schlutz, L., Hellstern, E. and Urban, K.: Glass forming range in mechanicallyalloy ed NiZr and the influence of the milling intensity. J Appl Phys, 64, 3224. (1998).
[12.] Essl, F., Bruhn, J., Janssen, R. and Claussen, N.: Wet milling of Al-containing powder mixtures as precursor materials for reaction bonding of alumina (RBAO) and reaction sintering of aluminium-aluminide alloys (3A). Materials Chemistry and Physics, 61, 69-77. (1999).
[13.] Fredriksson, R., Rosén, E. and Kullgren, A.: Priorities of pedestrian protection– A real-life study of severe injuries and car sources. Accident Analysis &Prevention, 42(6), 1672-1681. (2010).
[14.] Hanna, W., Maung, K., El-Danaf, E. A., Almajid, A. A., Soliman, M. S. and Mohamed, F. A.: Nanocrystalline 6061 Al Powder Fabricated by Cryogenic Milling and Consolidated via High Frequency Induction Heat Sintering. Advances in Materials Science and Engineering, 2014, 1-9. (2014).
[15.] Hassan, S. B., Agunsoye, J. O. and Bello, S. A.: Ball Milling Synthesis of Al (1050) Particles: Morphological Study and Particle Size Determination. Industrial Engineering Letters, 5(11), 22-27. (2015).
[16.] Janot, R. and Guérard, D.: Ball-milling in liquid media: Applications to the preparation of anodic materials for lithium-ion batteries. Progress in Materials Science, 50(1), 1-92. (2005).
[17.] Knieke, C., Steinborn, C., Romeis, S., Peukert, W., Breitung-Faes, S. and Kwade, A.: Nanoparticle Production with Stirred-Media Mills: Opportunities and Limits. Chemical Engineering & Technology, 33(9), 1401-1411. (2010).
[18.] Kwade, A.: Wet comminution in stirred media mills — research and its practical application. Powder Technology, 105 14-20. (1999).
[19.] Li, J., Li, F., Hu, K. and Zhou, Y.: TiB2/TiC nanocomposite powder fabricated via high energy ball milling. Journal of the European Ceramic Society, 21(16), 2829-2833. (2001).
[20.] Liu, T., Shen, H., Wang, C. and Chou, W.: Structure evolution of Y2O3 nanoparticle/Fe composite during mechanical milling and annealing. Progress in Natural Science: Materials International, 23(4), 434-439. (2013).
[21.] Loh, Z. H., Samanta, A. K. and Sia Heng, P. W.: Overview of milling techniques for improving the solubility of poorly water-soluble drugs. Asian Journal of Pharmaceutical Sciences, 10(4), 255-274. (2015).
[22.] Maurice, D. R. and Courtney, T. H.: The physics of mechanical alloying: a first report. Met Trans A, 21, 289-303. (1990).

[23.] Mazaheri, Y., Karimzadeh, F. and Enayati, M. H.: Nanoindentation Study of Al356-Al2O3 Nanocomposite Prepared by Ball Milling. Materials Sciences and Applications, 01(04), 217-222. (2010).
[24.] Mohamed, F. A.: A dislocation model for the minimum grain size obtainable by milling. Acta Materialia, 51(14,), 4107-4119. (2003).
[25.] Perez, N.: Fracture Mechanics (1 ed. Vol.US: Springer.(2004)
[26.] Pokropivny, V., Lohmus, R., Hussainova, I., Pokropivny, A. and Vlassov, S. (2007). Introduction to nanomaterials and nanotechnology (pp. 192): Tartu University Press, www.tyk.
[27.] Prasad Yadav, T., Manohar Yadav, R. and Pratap Singh, D.: Mechanical Milling: a Top Down Approach for the Synthesis of Nanomaterials and Nanocomposites. Nanoscience and Nanotechnology, 2(3), 22-48. (2012).
[28.] Qu, Y., Luo, H., Li, H. and Xu, J.: Comparison on structural modification of industrial lignin by wet ball milling and ionic liquid pretreatment. Biotechnology Reports, 6, 1-7. (2015).
[29.] Shonhiwa, A., Herrmann, M., Sigalas, I. and Coville, N.: Reaction bonded aluminum oxide composites containing cubic boron nitride. Ceramics International, 35(2), 909-911. (2009).
[30.] Speakman, C. A. ([n,d]). Estimating Crystallite Size Using XRD (pp. 1-105): MIT Center for Materials Science and Engineering.
[31.] The United Kingdom composites Industry: The United Kingdom composites industry – turning ideas into investments. Reinforced Plastics, 57(3), 43-46. (2013).
[32.] Watson, M. J., Chan, H. M., Harmer, M. P. and Caram, H. S.: Effects of Milling Liquid on the Reaction-Bonded Aluminum Oxide Process. J. Am. Ceram. Soc., 81(8), 2053-2060. (1998).
[33.] Wolff, M. F. H., Antonyuk, S., Heinrich, S. and Schneider, G. A.: Attritor-milling of poly(amide imide) suspensions. Particuology, 17, 92-96. (2014).
[34.] Yang, F., Yan, G., Wang, Q. Y., Xiong, X. M., Li, S. Q., Liu, G. Q., Zhang, P. X.: The Effect of High-energy Ball Milling on the Microstructure and Properties of Ti-doped MgB2 Bulks and Wires. Physics Procedia, 65, 157-160. (2015).
[35.] Zhang, S., Liu, J., Feng, J., Li, C., Ma, X. and Zhang, P.: Optimization of FeSe superconductors with the high-energy ball milling aided sintering process. Journal of Materiomics, 1(2), 118-123. (2015).
[36.] Zhang, X., Mu, H., Huang, X., Fu, Z., Zhu, D. and Ding, H.: Cryogenic Milling of Aluminium-lithium Alloys: Thermo-mechanical Modelling towards Fine-tuning of Part Surface Residual Stress. Procedia CIRP, 31, 160-165. (2015).